Preprint typeset using LaTeX style emulateapj v. 14/09/00

THE DIVERSITY OF HIGH- AND INTERMEDIATE-VELOCITY CLOUDS: COMPLEX C VERSUS IV ARCH[1]

Philipp Richter[2], Kenneth R. Sembach[3], Bart P. Wakker[2], Blair. D. Savage[2], Todd M. Tripp[4], Edward M. Murphy[3], Peter M.W. Kalberla[5]
and
Edward B. Jenkins[4]

ABSTRACT

We present *Far Ultraviolet Spectroscopic Explorer* (FUSE) and *Space Telescope Imaging Spectrograph* (STIS) observations of interstellar ultraviolet absorption lines in the Galactic high-velocity cloud Complex C and the Intermediate Velocity Arch (IV Arch) in direction of the quasar PG 1259+593 ($l = 120.^\circ6$, $b = +58.^\circ1$). Absorption lines from C II, N I, N II, O I, Al II, Si II, P II, S II, Ar I, Fe II, and Fe III are used to study the atomic abundances in these two halo clouds at $V_{\rm LSR} \sim -130$ km s^{-1} (Complex C) and -55 km s^{-1} (IV Arch). The O I/H I ratio provides the best measure of the overall metallicity in the diffuse interstellar medium, because ionization effects do not alter the ratio, and oxygen is at most only lightly depleted from the gas into dust grains. For Complex C, we find an oxygen abundance of $0.093\ ^{+0.125}_{-0.047}$ solar, consistent with the idea that Complex C represents the infall of low metallicity gas onto the Milky Way. In contrast, the oxygen abundance in the IV Arch is $0.98\ ^{+1.21}_{-0.46}$ solar, which indicates a Galactic origin. We report the detection of an intermediate-velocity absorption component at +60 km s^{-1} that is not seen in H I 21 cm emission. The clouds along the PG 1259+593 sight line have a variety of properties, proving that multiple processes are responsible for the creation and circulation of intermediate- and high-velocity gas in the Milky Way halo.

Subject headings: ISM: clouds – ISM: abundances – quasars: absorption lines – quasars: individual (PG 1259+593) – Galaxy: halo

1. INTRODUCTION

Although significant progress has been made in the last few years in exploring the distribution and chemical composition of intermediate and high-velocity clouds (IVCs and HVCs, respectively) in the halo of the Milky Way, an overall unified model for their formation is still lacking. These clouds are typically defined as concentrations of neutral hydrogen (H I) at velocities inconsistent with a simple model of differential Galactic rotation. The distinction between IVCs and HVCs is loosely based on the observed radial velocities of the clouds; IVCs have radial velocities with respect to the Local Standard of Rest (LSR) of 30 km s^{-1} $\leq |V_{\rm LSR}| \leq$ 90 km s^{-1}, while HVCs have velocities $|V_{\rm LSR}| >$ 90 km s^{-1}. Recent studies (Lu et al. 1998; Wakker et al. 1999; Gibson et al. 2000, 2001; Murphy et al. 2000; Bluhm et al. 2001; Sembach et al. 2001) reveal disparate chemical compositions for several of these clouds in different directions in the sky. The kinematics and chemical make-up of the IVCs and some of the HVCs can be explained successfully by the "Galactic fountain" model (Shapiro & Field 1976; Houck & Bregman 1990), in which hot gas ejected out of the Galactic disk by supernova explosions eventually falls back in the form of condensed neutral clouds moving at intermediate and high velocities. Clouds participating in this circulatory pattern should have a nearly solar metallicity reflecting that of their place of origin. There are, however, a number of HVCs whose abundances are inconsistent with the Galactic fountain model. One such case is the Magellanic Stream, which has abundances close to those of the Small Magellanic Cloud (SMC) and is believed to be tidally stripped out of the SMC system during a close encounter with the Galaxy (e.g., Wannier & Wrixon 1972; Lu et al. 1998; Gibson et al. 2000; Sembach et al. 2001). High-velocity cloud Complex C has an even lower abundance ($\sim$ 0.1 solar; Wakker et al. 1999) that is inconsistent with gas originating in the disk of the Galaxy or in the Magellanic Clouds. Thus, Complex C might represent accreting metal-poor material from intergalactic space. Accretion of substantial quantities of metal-poor gas in the form of HVCs would have a significant influence on the chemical evolution of the Milky Way.

It is clear that all of the intermediate and high-velocity clouds in the Galactic halo do not have a single common origin. Therefore, it is important to quantify the properties of IVCs and HVCs to the greatest extent possible using ultraviolet (UV) absorption line spectroscopy. Many astrophysically important atoms and molecules have their electronic transitions in the wavelength region between 912

[1] Partly based on observations with the NASA/ESA Hubble Space Telescope, obtained at the Space Telescope Science Institute, which is operated by the Association of Universities for Research in Astronomy, INC. under NASA contract NAS5-26555.

[2] Department of Astronomy, University of Wisconsin-Madison, 475 N. Charter Street, Madison, WI 53706; richter@astro.wisc.edu

[3] Department of Physics and Astronomy, Johns Hopkins University, 3400 N. Charles Street, Baltimore MD 21218

[4] Princeton University Observatory, Peyton Hall, Princeton, NJ 08544

[5] Radioastronomisches Institut, Universität Bonn, 53121 Bonn, Germany

and 3000 Å. Ultraviolet absorption line spectroscopy is the most sensitive and accurate method to study gas-phase abundances and physical properties in diffuse interstellar clouds in the Galactic halo, where typical gas densities are significantly lower than in Galactic disk clouds. The *Far Ultraviolet Spectroscopic Explorer* (FUSE) has sufficient sensitivity and spectral resolution to investigate absorption at $\lambda \leq 1187$ Å in the Galactic halo and beyond along a large number of sight lines. At longer wavelengths ($\lambda > 1150$ Å), the *Space Telescope Imaging Spectrograph* (STIS) on HST provides additional information for a number of atomic species and the Lyα absorption line of neutral hydrogen near 1215.7 Å. Combining data from these instruments provides a particulary powerful tool for investigating HVCs and IVCs.

In this study we use FUSE and STIS absorption line data to investigate the intermediate- and high-velocity gas in the Galactic halo toward the quasar PG 1259+593 ($V = 15.84$; $z_{\rm em} = 0.478$; $l = 120\fdg6$, $b = +58\fdg1$). This sight line passes through the Intermediate-Velocity Arch (IV Arch; Kuntz & Danly 1996) and the high-velocity cloud Complex C (see Wakker & van Woerden 1997). Complex C has been the subject of several recent absorption line studies along different lines of sight. For example, Wakker et al. (1999) studied the sulfur abundance of Complex C toward Mrk 290 and found (S/H) $= 0.089 \pm 0.024\,(^{+0.020}_{-0.005})$ solar based on UV absorption line data in combination with high resolution H I data from the Westerbork Radio Telescope and Hα data from the *Wisconsin Hα Mapper* (WHAM). In contrast, Murphy et al.(2000) observed Mrk 876 with FUSE and found (Fe II/H I) $= 0.48 \pm 0.2(\pm 0.2)$ times the solar (Fe/H) ratio in Complex C, suggesting little or no depletion of Fe into dust grains. Gibson et al. (2001) analyzed STIS data of the Complex C absorption along the sight lines toward Mrk 279, Mrk 290, Mrk 501, Mrk 817, and Mrk 876, and found variations in S II/H I implying (S/H) in the range from 0.08 to 0.44 solar. These variations could be due in part to ionization effects, although intrinsic abundance variations within Complex C cannot be ruled out.

To avoid having to deal with substantial ionization corrections, we have chosen to study the metal content in Complex C toward PG 1259+593. The sight line passes through Complex C in a region of relatively high H I column density ($(8.4 \pm 0.1) \times 10^{19}$ cm^{-2}; Wakker et al. 2001), so ionization effects are much less important than at lower column densities. Other Complex C sight lines either have much lower UV fluxes (e.g., Mrk 290) or substantially lower column densities and greater confusion with lower velocity features (e.g., Mrk 279, Mrk 876). In the direction of PG 1259+593, the Complex C absorption is well-separated in velocity from the IV Arch, thus allowing a direct comparison of intermediate and high-velocity material in the Galactic halo *within the same spectrum*. The IV Arch lies at a height of $0.8-1.5$ kpc above the Galactic plane (see Wakker 2001). An overall metallicity for the IV Arch has yet not been well determined, although several sulfur measurements (Spitzer & Fitzpatrick 1993; Fabian et al., in preparation) suggest a near-solar metallicity, in striking contrast to the much lower metallicity of the more distant Complex C (d > 6.1 kpc; van Woerden et al. 1999). An extensive summary of absorption line measurements available for many IVCs and HVCs is given by Wakker (2001).

This paper is organized as follows: we review the sight line structure toward PG 1259+593 in §2. In §3 we present the FUSE and STIS observations of PG 1259+593 and our analysis methods. In §4 we discuss absorption from gas associated with Complex C; in §5 we analyze absorption related to the IV Arch. In §6 we report the discovery of another IVC component at positive velocities. §7 provides a brief summary of the velocity distribution of the highly ionized species observed along the sight line. Concluding remarks are given in §8.

2. THE PG 1259+593 SIGHT LINE

The H I emission lines of the PG 1259+593 sight line as observed with the Effelsberg 100m telescope (Wakker et al. 2001; 9.′1 beam), the NRAO 140 foot telescope at Green Bank (Murphy et al., in preparation; 21.′0 beam), and the Leiden-Dwingeloo Survey (Hartmann & Burton 1997; 36.′0 beam) are shown in the left panel of Figure 1. Three major H I components are visible at 0, -55 and -130 km s^{-1}, representing emission from local Galactic gas, the IV Arch close to core IV 19 (Kuntz & Danly 1996) in the lower Galactic halo, and high-velocity cloud Complex C near the CIII-C core (Giovanelli, Verschuur & Cram 1973), respectively. The local Galactic H I emission component is weak because the direction $l = 120\fdg6$, $b = 58\fdg1$ lies close to the "Lockman Hole", the region with the smallest amount of local H I in the northern hemisphere (Lockman, Jahoda, & McCammon 1986). This makes the analysis of the intermediate- and high-velocity material along this sight-line less complicated than in other directions because 1) the local component is not confused with absorption at intermediate velocities, and 2) local H_2 absorption, which can blanket a significant portion of the UV spectrum below ~ 1100 Å, is weak. There are substantial differences in the three H I emission profiles shown in Figure 1 resulting from the different instrumental resolutions of the data and beam-smearing effects. We adopt the highest resolution (Effelsberg) data, yielding N(H I) $= (4.4 \pm 0.5) \times 10^{19}$ cm^{-2} for the local Galactic component at 0 km s^{-1}, $(3.0 \pm 0.1) \times 10^{19}$ cm^{-2} for the IV Arch at -55 km s^{-1}, and $(8.4 \pm 0.1) \times 10^{19}$ cm^{-2} for Complex C at -130 km s^{-1} (Wakker et al. 2001). [6]

PG 1259+593 has a redshift of $z_{\rm em} = 0.478$ (Marziani et al. 1996), and there are several intergalactic H I Ly α absorbers along this sight line (e.g., Bahcall et al. 1993). Intergalactic absorption detected in the FUSE and STIS data will be discussed in a future paper. For the present study, it is sufficient to note that these IGM features do not affect the analysis of the absorption associated with Complex C and the IV Arch presented in this paper.

[6] The H I column densities derived from the lower resolution data are $(4.9 \pm 1.9) \times 10^{19}$ cm^{-2} (Green Bank; GB) and $(3.6 \pm 0.5) \times 10^{19}$ cm^{-2} (Leiden-Dwingeloo; LD) for the local Galactic component, $(3.6 \pm 1.5) \times 10^{19}$ cm^{-2} (GB) and $(2.9 \pm 0.4) \times 10^{19}$ cm^{-2} (LD) for the IV Arch, and $(6.3 \pm 1.6) \times 10^{19}$ cm^{-2} (GB) and $(4.1 \pm 0.4) \times 10^{19}$ cm^{-2} (LD) for Complex C.

3. OBSERVATIONS AND DATA REDUCTION

FUSE is equipped with four co-aligned optical channels (2 SiC channels for 905-1105 Å and 2 LiF channels for 1000-1187 Å) and two microchannel plate detectors. A detailed description of the FUSE instrument and its on-orbit performance is given by Moos et al. (2000) and Sahnow et al. (2000). The FUSE observations of PG 1259+593 were obtained on 25 February 2000, 25 December 2000, and 29 January 2001 through the large apertures (LWRS, $30'' \times 30''$) of the four channels and were recorded in photon address mode. Sixty-four exposures totaling ~ 193 ks. are available for all four channels, although the light of the quasar was not optimally centered in all of the apertures throughout the observations and the detector high voltage was down during part of one observation. Table 1 provides an overview of the FUSE observations of PG 1259+593. A detailed analysis of the raw time-tagged photon list was required to eliminate small event bursts of unknown origin from the raw data (see Sahnow et al. 2000).

The data were extracted using the standard FUSE calibration pipeline CALFUSE (v1.8.7) available at the Johns Hopkins University, and the individual exposures for each channel were coadded using a cross-correlation technique to remove small relative wavelength shifts between exposures. The pipeline corrects for geometrical distortions in the detector grid, the Doppler shifts introduced by the motions of Earth and satellite through space, and small spectral shifts due to thermally-induced motions of the diffraction gratings. This version of the pipeline does not correct for fixed-pattern noise or the spatial curvature of the lines introduced by the astigmatism of the optical system, which degrades the spectral resolution slightly at most wavelengths. To improve the signal-to-noise ratio (S/N), the data were rebinned over 5 pixels, resulting in ~ 10 km s^{-1} wide bins. No additional smoothing was applied. The velocity resolution of the combined FUSE data is ~ 25 km s^{-1} (FWHM). The average flux in the spectrum is $\sim 2 \times 10^{-14}$ erg cm^{-2} s^{-1} Å^{-1}, equivalent to an average S/N of ~ 10 per (rebinned) pixel element.

STIS observations of PG1259+593 were carried out on 17–19 January 2001 with the intermediate-resolution far-UV echelle grating (E140M) and the $0.''2 \times 0.''06$ slit. Thirty-four exposures totaling 81 ksec were obtained. In this observing mode, STIS provides a resolution of 7 km s^{-1} (FWHM) and wavelength coverage from ∼1150 to 1730 Å with only five small gaps between orders at $\lambda >$ 1634 Å. We reduced the data with the STIS Investigation Definition Team (IDT) version of CALSTIS at the Goddard Space Flight Center. The individual spectra were flatfielded, extracted, and wavelength and flux calibrated with the standard procedures. The STIS IDT correction for scattered light was then applied, and the individual spectra were co-added weighted by their inverse variances averaged over a large, high signal-to-noise region. Finally, overlapping regions of adjacent orders were co-added with weighting based on inverse variance. For further information on the design and on-orbit performance of STIS, see Woodgate et al. (1998) and Kimble et al. (1998).

The FUSE and STIS absorption profiles were continuum-normalized by fitting low-order polynomials to the data; a selection of normalized profiles is shown in Figure. 1. (For display purposes only, we have rebinned the STIS data in this figure to ~ 10 km s^{-1} wide pixel elements, similar to the FUSE data.) We measured equivalent widths for the weakly ionized species in the HVC and IVC gas by fitting single Gaussian profiles to the main absorption components at -130 km s^{-1} (Complex C), -55 km s^{-1} (IV Arch), and for the IVC at $+60$ km s^{-1}. For every line in the FUSE bandpass, equivalent widths were measured independently using data for the two highest S/N channels, and then the values were averaged with weights proportional to the inverse squares of the respective errors. Wavelengths, oscillator strengths (Morton 1991; 2001, in preparation), and equivalent widths (and 1σ errors) for all measured lines are listed in Table 2. The cited errors include contributions from photon statistics and continuum placement uncertainties. For the determination of column densities we made use of a standard curve-of-growth technique.

4. COMPLEX C

Metal line absorption from weakly ionized species associated with Complex C is detected near -130 km s^{-1} in C II, C III, N I, O I, Al II, Si II, S II, and Fe II. Weak lines from other species (e.g., Ar I λ1048.220 and P II λ1152.818) are not detected at Complex C velocities, but 3σ upper limits were derived (see Table 2). Measurements of the equivalent widths of C II, C III, and Si III in Complex C are not possible since these strong lines extend over the entire velocity range between -180 to $+180$ km s^{-1} (see Figure 1). The strong lines of oxygen, silicon, and iron exhibit an asymmetry in the red wing of their absorption profiles, implying the presence of a weak absorption component near -110 km s^{-1}. Multiple Complex C components have also been observed toward other background sources (e.g., Mrk 876, see Gibson et al. 2001), where H I emission and absorption by weakly ionized species arises in at least two distinct components between -100 and -200 km s^{-1}. The present PG 1259+593 data do not allow us to analyze the two absorptions separately for all species, so we will consider the effect of this weak component on our column density determinations by examining its effect on the O I and Si II lines observed by STIS. The present Effelsberg H I 21cm emission data do not give any guidance as to the existence of multiple H I emission components, but it is possible to include a narrow, weak ($\log N(\mathrm{H\ I}) < 18.5$) emission component at ~ -110 km s^{-1} without a noticeable change in the observed profile.

All of the Complex C lines from weakly ionized species collectively fit a single-component curve of growth with $b = 9.8^{+4.7}_{-1.2}$ km s^{-1} (Figure 2), suggesting that the velocity-dispersion parameter is determined by turbulent motions. There is a systematic trend for the stronger lines (e.g., O I λ1302.169) to favor a higher b-value than the weak lines, supporting the idea that in this direction Complex C consists of two or more unresolved subcomponents. Column densities and gas-phase abundances relative to the solar values (Anders & Grevesse 1989; Grevesse & Noels 1993) were derived by fitting the data to a single-component curve of growth with $b = 9.8$ km s^{-1}; they are presented in Table 3 along with their respective 1σ errors.

To estimate the influence of a possible unresolved subcomponent at ~ -110 km s^{-1} on the Complex C column densities, we have created composite apparent column den-

sity profiles (see Savage & Sembach 1991) for the strong absorption lines of oxygen and silicon in the STIS data. A weak component at -114 km s^{-1} is clearly visible. Simulating the influence of this component on the overall Complex C line profile, we find that such a component modifies the curve of growth of the main component in a very gentle manner, and the resulting curve is very similar to the curve of growth with $b = 9.8$ km s^{-1}, derived from our single-component Gaussian fitting analysis. We estimate an uncertainty of ≈ 0.05 dex (12%) for the abundances in Complex C due to the existence of this unresolved absorption component (note that this uncertainty is not included in the formal errors cited in Table 3). The presence of this subcomponent does not significantly alter the conclusions of our abundance study of Complex C.

All elements considered in this study have normalized gas-phase abundances defined by $[X/\mathrm{H}] \equiv \log(N_X/N_{\mathrm{H\,I}}) - \log(X/\mathrm{H})_\odot < -0.8$ dex, except phosphorus, for which only a 3σ upper limit of ≤ -0.27 could be derived. Comments regarding the limits for Ar I and Fe II are found in subsequent paragraphs. The normalized interstellar gas-phase abundances for all measured species in Complex C are shown in Figure 3. An accurate measure for the mean metallicity in the ISM is the O I/H I ratio; oxygen is not significantly depleted onto dust grains (Meyer et al. 1998) and the O I/H I ratio is not altered by ionization effects (i.e., (O I/H I) $\approx$ (O/H)). This is because O I and H I have similar ionization potentials and both elements are strongly coupled through charge exchange interactions (e.g., Sofia & Jenkins 1998). For Complex C, we find $[\mathrm{O/H}] = -1.03^{+0.37}_{-0.31}$, equivalent to $0.093^{+0.125}_{-0.047}$ times the solar (O/H) ratio. The value agrees very well with the low sulfur abundance found toward Mrk 290 (Wakker et al. 1999), but is significantly lower than the sulfur and iron abundances derived from S II and Fe II toward Mrk 279, Mrk 501, Mrk 817, and Mrk 876 (Gibson et al. 2001; Murphy et al. 2000). For S II we find $[\mathrm{S/H}] = -0.85^{+0.12}_{-0.15}$. Thus, the inferred normalized gas-phase abundance of sulfur is significantly higher than for oxygen, but S II exists in regions were hydrogen is both neutral and ionized. Assuming that the sulfur-to-oxygen ratio in Complex C is the same as in local Galactic gas and that the residual difference in the measured values is caused by S II in ionized gas along the sight line, we estimate an average degree of ionization of $\mathrm{H^+/(H^0+H^+)} = 0.32$ and $N(\mathrm{H_{total}}) = N(\mathrm{H^0}) + N(\mathrm{H^+}) = 1.26 \times 10^{20}$ cm^{-2}. [7]

If UV radiation is the major source of ionization in Complex C, it would be straight forward to explain the nondetection of neutral argon because Ar I has a large photoionization cross section (Sofia & Jenkins 1998). Comparing Ar I to H I, we find $[\mathrm{Ar/H}] \leq -1.42$, but it is possible that the actual value for [Ar/H] is significantly *higher*, if most of the Ar is in the form of Ar II. For similar reasons, a significant fraction of the nitrogen may also be ionized, which could account for the very low normalized abundance based on N I ($[\mathrm{N/H}] = -1.94^{+0.17}_{-0.21}$). The N II λ1083.994 absorption profile observable with FUSE is consistent with a strength of $\sim$ 130 mÅ required to correct the the total nitrogen abundance up to 0.1 solar. However, this line has low S/N and it is blended by Fe II λ1083.420. We derive an upper limit of 183 mÅ (3σ) for N II absorption at Complex C velocities.

Although the normalized gas-phase abundances derived for O, Al, Si, S, and Fe are consistent with a single value to within the errors, the data show weak evidence for a slight underabundance of iron in comparison to the other elements. We find $[\mathrm{Si/H}] = -0.91^{+0.28}_{-0.27}$ and $[\mathrm{Al/H}] = -0.98^{+0.30}_{-0.50}$, and $[\mathrm{Fe/H}] = -1.27^{+0.20}_{-0.14}$, based on the data for Si II, Al II, and Fe II. The abundance of Al is derived from a single saturated line (Al II λ1670.787) and therefore has a relatively large error bar. In the local interstellar medium, Si, Al, and Fe are all depleted into dust grains and their gas-phase abundance is significantly lower than that of mildly depleted species, such as O (e.g., Savage & Sembach 1996). For Complex C, however, we find [Si/H]$\approx$[Al/H]$\approx$[O/H], indicating that silicon and aluminum are probably not incorporated into dust grains in Complex C if the ionization corrections for Si II and Al II are modest. While the ionization potentials for Si II and Fe II are almost identical, the photoionization cross section of Fe II is much higher than that of Si II once the ionizing photons exceed an energy of $\sim$ 20 eV (see Figure 3 in Sofia & Jenkins 1998). Thus, its appears plausible that a significant fraction of the missing iron is in Fe III because of ionizing radiation at high energies.

We can check on the amounts of doubly ionized species in Complex C. Si III λ1206.500 absorption is present at Complex C velocities in the STIS spectrum, but this line cannot be used to derive a Si III column density because the three velocity components are heavily overlapping (see Figure 1). The Fe III λ1122.524 line is observed by FUSE but it is blended by Galactic Fe II λ1121.975 (Figure 1). Estimating the strength of the blending Fe II λ1121.975 absorption by comparing with Fe II λ1096.877 (the two lines have similar values of log $f\lambda$ – see Table 2) yields a Galactic Fe II component strength of $\approx$ 50 mÅ. The equivalent width of Galactic Fe II λ1121.975 plus Fe III λ1122.524 at -130 km s^{-1} has a very similar strength, suggesting that there is no significant Fe III absorption at Complex C velocities ($<$ 33 mÅ (3σ)). We derive log N(Fe III)$\leq$ 13.67 and [(Fe II+Fe III)/H I] = -1.15, or 0.24 dex lower than [Si/H] based solely on Si II. Therefore, the apparently low abundance of iron in Complex C is not likely to result from ionization effects. More likely, a low iron abundance in Complex C could be due to depletion of iron into Fe-rich dust grains. As discussed by Savage & Sembach (1996), dust-phase abundance measurements of Galactic halo clouds indicate the presence of dust cores that contain Mg and Fe but do not contain much Si. An alternative, and perhaps more speculative hypothesis, would be that a low iron abundance in Complex C reflects an overabundance of α elements (S, Si, and O) compared to iron. An enhanced abundance of α elements in Complex C has also been suggested for the Mrk 876, Mrk 290, and Mrk 817 sight lines based upon comparisons of N I, S II, and Fe II column densities (Gibson et al. 2001; Murphy et al. 2000). However, considering that the abundances of iron and other elements are consistent *within their error range*, more accurate data is required to investigate the apparent iron deficiency in Complex C on a statistically

[7] We note that the S/O ratio in Complex C might differ from the solar value because of a different nucleosynthetic history. If so, the ionization fraction would be different.

more reliable basis.

Summarizing, we find that Complex C has an overall abundance of ∼0.1 solar in the direction of PG 1259+593, strongly supporting the idea that Complex C has an origin outside the Milky Way. Additional high quality data for other sight lines may help to quantify the abundance pattern in Complex C and determine whether the apparent abundance variations seen in Complex C by Gibson et al. (2001) and the apparent iron deficiency toward PG 1259+593 are intrinsic in nature or due to a combination of effects (e.g., nucleosynthetic history, ionization, dust).

5. IV ARCH

Absorption lines of weakly ionized metals C II, C III, N I, O I, Al II, Si II, Si III, S II, and Fe II are detected at the velocity of the IV Arch (-55 km s^{-1}). Absorption lines of Ar I and P II are not detected. The equivalent widths are listed in Table 2. The data fit best on a curve of growth with $b = 10.2^{+5.7}_{-3.2}$ km s^{-1} (Figure 2), implying macroscopic turbulence and/or unresolved sub-components. Column densities and gas-phase abundances, based on the single component fit to the curve of growth with $b = 10.2$ km s^{-1}, are presented in Table 3. Figure 3 provides an overview of normalized interstellar gas-phase abundances in the IV Arch (see also §4). The oxygen abundance in the IV Arch is [O/H]$= -0.01^{+0.35}_{-0.27}$, or $0.98^{+1.21}_{-0.46}$ solar, in striking contrast to the low oxygen abundance for Complex C derived in the previous section. The sulfur abundance (derived from S II) is slightly higher, [S/H]$= +0.11^{+0.11}_{-0.08}$, suggesting an ionization fraction of $H^+/(H^0+H^+) = 0.24$ using the same line of reasoning in §4. Similar to Complex C, argon and nitrogen are very underabundant in comparison to oxygen and sulfur ([Ar/H]≤ -0.98 and [N/H]$= -0.68^{+0.50}_{-0.29}$, based on the data for Ar I and N I). These low abundances are most likely due to photoionization since neither argon nor nitrogen is readily incorporated into dust. Low argon and nitrogen abundances have been seen also in other intermediate-velocity clouds (e.g., Richter et al. 2001). Abundances for silicon (Si II) and iron (Fe II) are [Fe/H] $= -0.22^{+0.28}_{-0.33}$ dex and [Si/H] $= -0.26^{+0.19}_{-0.15}$, suggesting relatively mild depletions into dust grains.

The nearly solar abundances and the z-height bracket of $0.8 - 1.5$ kpc suggest that the IV Arch has its origin in the Milky Way disk, for instance as part of a Galactic fountain (Shapiro & Field 1976; Houck & Bregman 1990). The abundances derived here agree well with those for the LLIV Arch toward PG 0804+761 (Richter et al. 2001). The FUSE and STIS data of PG 1259+593 therefore suggest that the IV Arch and Complex C have completely different origins.

6. IVC AT $+60$ KM S^{-1}

The strong absorption lines of O I, C II, C III, Al II, Si II, Si III, and Fe II reveal the presence of another IVC component at *positive* velocities near $+60$ km s^{-1}. Absorption at positive velocities is not expected for interstellar gas participating in Galactic rotation in this direction. Equivalent widths for this absorption component are listed in Table 2. Neither the Effelsberg nor the Green Bank H I data show emission at $+60$ km s^{-1}, suggesting that the H I column density is below the detection limit. Another possibility is that the diameter of this cloud is very small and that beam-smearing effects make this component undetectable in H I emission. The Effelsberg data yield a 3σ upper limit of $N(\mathrm{H\,I}) \leq 3.0 \times 10^{18}$ cm^{-2} for this IVC. H I absorption in the higher Lyman lines (Ly γ and higher) may be present, but blending with the Galactic H I component and other lines in combination with low S/N at these wavelengths prevents any useful quantitative analysis of the H I absorption. Thus, it is impossible to determine abundances for this IVC with the present data.

7. HIGHLY IONIZED SPECIES

In addition to the weakly ionized species, absorption lines of C IV λ1548.195, Si IV λ1393.755, and O VI λ1031.926 are seen in both Complex C and the IV Arch. This is the second detection of O VI in Complex C (see Murphy et al. 2000 for the profiles toward Mrk 876). The O VI absorption profile is shown in Figure. 1. O VI absorption at negative velocities might also be present in the other O VI line at λ1037.617, but is blended by Galactic $H_2\,(5-0)\,R(1)$. The high ion absorption at Complex C velocities suggests the presence of a highly ionized boundary of Complex C caused by interaction with surrounding material in the Galactic halo (e.g., Sembach et al. 2000; Murphy et al. 2000).

8. CONCLUDING REMARKS

The FUSE spectrum of PG 1259+593 shows the diverse nature of intermediate- and high-velocity clouds in the halo of the Milky Way. Absorption line data obtained so far suggest that IVCs generally tend to have abundances similar to those in the disk of the Milky Way (for a summary see Wakker 2001) . Abundances found in HVCs, in contrast, are not explainable by a single origin. Metallicities of ~ 0.1 solar, as found for Complex C in this study and others (e.g., Wakker et al. 1999), indicate that metal-deficient gas is falling into the Milky Way halo. Other high-velocity clouds, such as the one in front of the LMC (Bluhm et al. 2001, Richter et al. in preparation), have significantly higher metal abundances, which can be explained by the Galactic fountain model. The Magellanic Stream (Lu et al. 1998; Gibson et al. 2000; Sembach et al. 2001) has abundances similar to that of the SMC and probably is the result of tidal interaction between the Milky Way and the SMC.

High-velocity cloud Complex C remains one of the most interesting cases of Galactic high-velocity gas investigated so far. Our [O/H] abundance for Complex C agrees well with the [S/H] abundance found by Wakker et al. (1999) toward Mrk 290, but studies of other sight lines suggest that there might be significant abundance variations in Complex C (Gibson et al. 2001; Murphy et al. 2000). The data obtained so far suggests that there might be a slight over-abundance of α elements in comparison to iron in Complex C. With this study, an abundance pattern including eight elements (N, O, Al, Si, P, S, Ar, and Fe) is now available for comparison with other sight lines. Further investigations of Complex C, in particular the study of its deuterium and molecular hydrogen content, may help to understand the abundances derived in this paper.

This work is based on data obtained for the the Guaranteed Time Team by the NASA-CNES-CSA FUSE mission operated by the Johns Hopkins University. Financial support has been provided by NASA contract NAS5-32985. Further support for this work was provided by NASA through grant number GO-08695.01-A from the Space Telescope Science Institute. KRS acknowledges partial support from NASA Long Term Space Astrophysics grant NAG5-3485. We thank J.C. Howk and W.P. Blair for helpful comments on this work.

REFERENCES

Anders, E., & Grevesse, N. 1989, Geochim. Cosmochim. Acta 53, 197
Bahcall, J.N., et al. 1993, ApJS, 87, 1
Bluhm, H., de Boer, K., Marggraf, O., & Richter, P. 2001, A&A, 367, 299
Gibson, B.K., Giroux, M.L., Penton, S.V., Putman, M.E., Stocke, J.T., & Shull, J.M. 2000, AJ, 120, 1830
Gibson, B.K., Penton, S.V., Giroux, M.L., Stocke, J.T., Shull, J.M., & Putman, M.E. 2001, AJ, submitted
Giovanelli, R., Verschuur, G. L., & Cram, T. R. 1973, A&AS, 12, 209
Grevesse, N., & Noels, A. 1993, in Orgin of the Elements, ed. N. Prantzos, E. Vangioni-Flam, & M. Cassé, (Cambridge: Univ. Press), 15
Hartmann, D., & Burton, W.B. 1997, Atlas of Galactic Neutral Hydrogen, Cambridge University Press
Houck, J.C., & Bregman, J.N. 1990, ApJ, 352, 506
Kimble, R. A., et al. 1998, ApJ, 492, L83
Kuntz, K.D., & Danly, L. 1996, ApJ, 457, 703
Lockman, F.J., Jahoda, K., & McCammon D. 1986, ApJ, 301, 380
Lu, L., Sargent, W.L.W., Savage, B.D., Wakker, B.P., Sembach, K.R., & Oosterloo, T.A. 1998, AJ, 115, 162
Marziani, P., Sulentic J.W., Dultzin-Hacyan, D., Calvani, M., & Moles, M. 1996, ApJS, 104, 37
Meyer, D.M., Jura, M., & Cardelli, J.A. 1998, ApJ, 493, 222
Moos, H.W., et al. 2000, ApJ, 538, L1
Murphy, E.M., Sembach, K.R., Gibson, B.K., et al. 2000, ApJ, 538, L35
Morton, D.C. 1991, ApJS, 77, 119
Richter, P., Savage, B.D., Wakker B.P., Sembach K.R., & Kalberla P.M.W. 2001, ApJ, 549, 281
Sahnow, D.J., et al. 2000, ApJ, 538, L7
Savage, B.D., & Sembach, K.R. 1991, ApJ, 379, 245
Savage, B.D., & Sembach, K.R. 1996, ARA&A, 34, 279
Sembach, K.R., Howk, J.C., Savage, B.D., & Shull, J.M. 2001, AJ, 121, 992
Sembach, K.R., et al. 2000, ApJ, 538, L31
Shapiro, P.R., & Field, G.B. 1976, ApJ, 205, 762
Sofia, U.J., & Jenkins, E.B. 1998, ApJ, 499, 951
Spitzer, E. L., & Fitzpatrick, E. L. 1993, ApJ, 409, 299
Wakker, B.P., & van Woerden, H. 1997, ARA&A, 35, 217
Wakker, B.P. 2001, ApJS, in press, astro-ph 0102147
Wakker, B.P., Kalberla, P.M.W., van Woerden, H., de Boer, K.S., & Putman M.E. 2001, ApJS, in press, astro-ph 0102148
Wakker, B.P., et al. 1999, Nature, 402, 388
Wannier, P., & Wrixon, G.T. 1972, ApJ, 173, L119
Woodgate, B. E., et al. 1998, PASP, 110, 1183
van Woerden, H., Peletier, R.F., Schwarz, U.J., Wakker, B.P., & Kalberla, P.M.W. 1999, in Stromlo Workshop on High-Velocity Clouds, eds. Gibson, B.K. & Putman, M.E., ASP Conf. Series Vol. 166, p.1

FIG. 1.— Continuum-normalized absorption profiles of several species from FUSE and STIS data of PG 1259+593, plotted against LSR velocity. For this plot, the data have been rebinned to 10 km s^{-1} wide pixels. The three major absorption components (local Galactic gas at 0 km s^{-1}, IV Arch at −55 km s^{-1}, and Complex C at −130 km s^{-1}) are marked with dotted lines and are identified above the boxes. Absorption at +60 km s^{-1} is visible only in the strong lines of C, O, Al, Si, and Fe. The three H I emission profiles (Effelsberg data with a 9.′1 beam, NRAO 140 ft. data with a 21.′0 beam, and Leiden-Dwingeloo data with a 36.′0 beam) show substantial differences, indicating beam smearing effects.

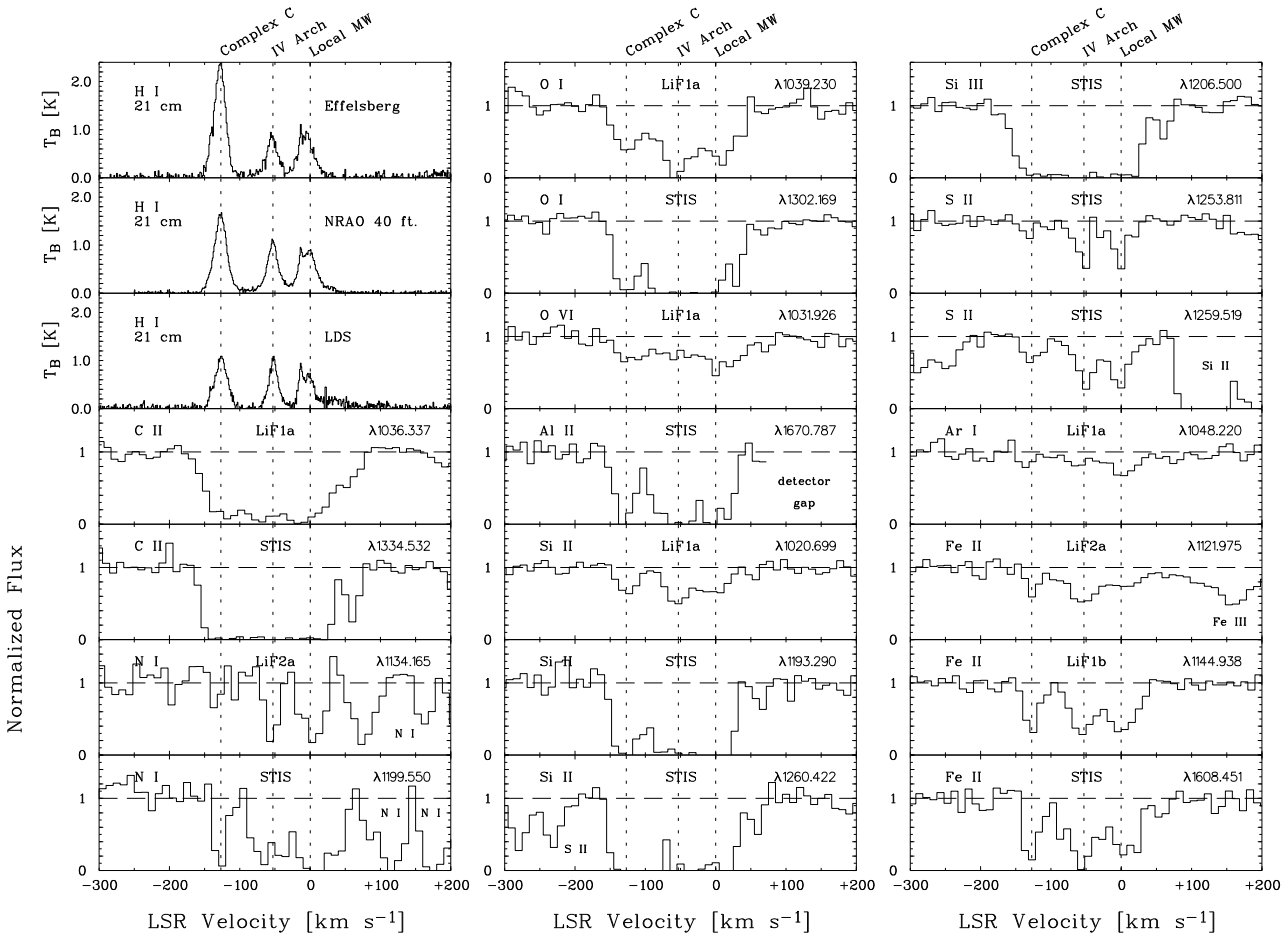

FIG. 2.— Empirical curves of growth for ions observed in Complex C (upper panel) and the IV Arch (lower panel). The different ions are labeled at the lower right side of each panel. For Complex C, the data points fit best on a curve of growth with $b = 9.8^{+4.7}_{-1.2}$ km s^{-1}. For the IV Arch, the best fit is found for $b = 10.2^{+5.7}_{-3.2}$ km s^{-1}.

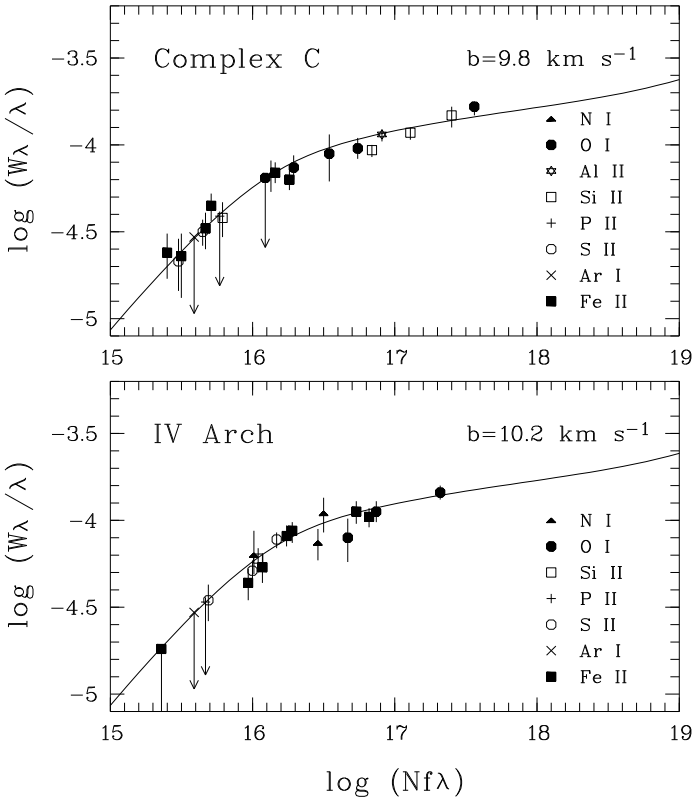

FIG. 3.— Normalized interstellar gas-phase abundances in Complex C and the IV Arch. Abundances in Complex C are systematically lower than in the IV Arch, suggesting a different enrichment history of both clouds. Ionization and dust depletion effects are discussed in §4 and §5. Error bars represent uncertainties from both equivalent-width measurement errors (see §3) and errors from the fits to the curves of growth.

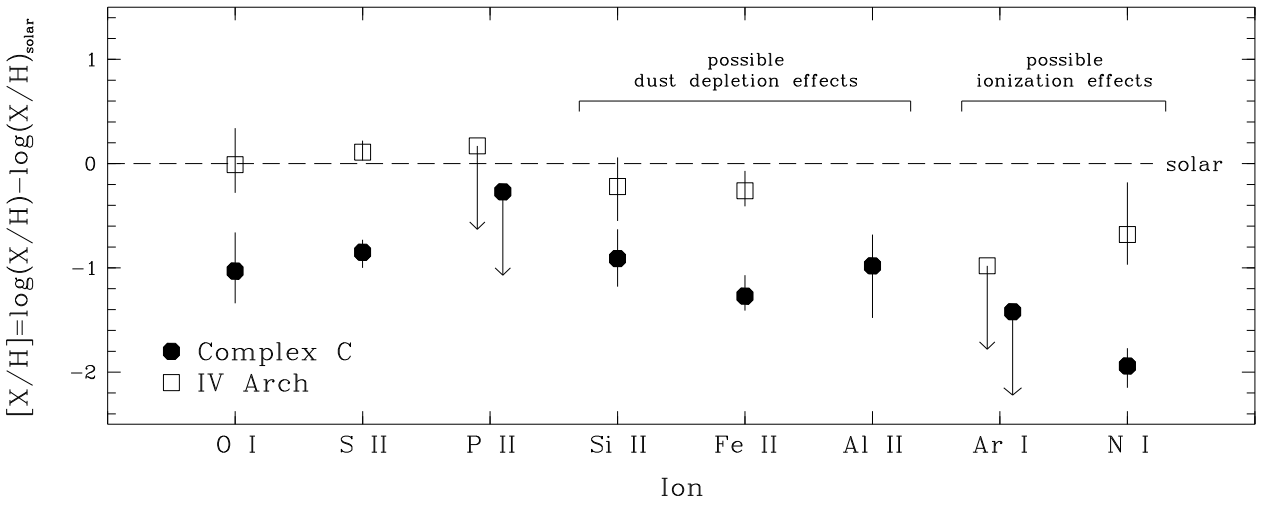

Table 1
Log of PG 1259+593 FUSE and STIS Observations

Instrument	Dataset ID	Obs. Date	Aperture	Exp. Time [ks]	Number of Exp.	Notes
FUSE	P1080101	2000 Feb. 25	$30'' \times 30''$	52.4	12	1
FUSE	P1080102	2000 Dec. 25	$30'' \times 30''$	57.9	21	2
FUSE	P1080103	2001 Jan. 29	$30'' \times 30''$	82.2	31	3
HST STIS	8695	2001 Jan. 17-19	$0\farcs2 \times 0\farcs06$	81.3	34	

Notes:

1) No SiC 2 channel data. SiC 1 and LiF 2 channels were not optimally centered at all times.

2) LiF 1 data only. SiC 1, SiC 2, and LiF 2 channels were not co-aligned - no flux recorded.

3) Detector 1 shut down during exposures 17-29.

Table 2
Atomic Absorption Lines Associated with Complex C, the IV Arch, and the IVC at +60 km s^{-1}

Species	λ_{vac} [a] [Å]	log λf [a]	$W_{\lambda\ ComplexC}$ [b] [mÅ]	$W_{\lambda\ IVArch}$ [b] [mÅ]	$W_{\lambda\ IV+60}$ [b] [mÅ]	Instrument
C II ...	1036.337	2.104	···	···	≤ 80	FUSE LiF1a, LiF2b
	1334.532	2.232	···	···	72 ± 9	HST STIS
N I	1134.165	1.238	≤ 41	72 ± 17	···	FUSE LiF2a
	1134.980	1.693	···	84 ± 17	···	FUSE LiF2a
	1199.550	2.202	81 ± 16	···	···	HST STIS
	1200.710	1.725	···	132 ± 30	···	HST STIS
N II ...	1083.994	2.097	≤ 183	···	···	FUSE SiC1a,SiC2b
O I	929.517	0.329	≤ 48	74 ± 22	···	FUSE SiC1b, SiC2a
	936.630	0.534	70 ± 11	106 ± 14	···	FUSE SiC1b,SiC2a
	948.686	0.778	84 ± 25	···	···	FUSE SiC2a
	1039.230	0.980	100 ± 13	151 ± 15	···	FUSE LiF1a, LiF2b
	1302.169	1.804	214 ± 20	···	22 ± 7	HST STIS
Al II ...	1670.787	3.486	186 ± 15	···	≤ 33	HST STIS
Si II ...	1020.699	1.225	39 ± 9	61 ± 10	···	FUSE LiF1a
	1190.416	2.543	···	···	24 ± 7	HST STIS
	1193.290	2.844	175 ± 25	···	29 ± 6	HST STIS
	1260.422	3.104	···	···	40 ± 7	HST STIS
	1304.370	2.284	121 ± 9	···	≤ 16	HST STIS
	1526.707	2.546	178 ± 13	···	···	HST STIS
Si III ..	1206.500	3.304	···	···	36 ± 6	HST STIS
P II ...	1152.818	2.451	≤ 37	≤ 37	···	FUSE LiF1b, LiF2a
S II	1250.584	0.834	≤ 19	43 ± 10	···	HST STIS
	1253.811	1.135	24 ± 8	64 ± 10	···	HST STIS
	1259.519	1.311	40 ± 7	97 ± 9	···	HST STIS
Ar I ...	1048.220	2.440	≤ 28	≤ 28	···	FUSE LiF1a, LiF2b
Fe II ...	1096.877	1.554	49 ± 9	95 ± 13	···	FUSE LiF2a
	1121.975	1.512	37 ± 9	92 ± 13	···	FUSE LiF1b, LiF2a
	1125.448	1.244	27 ± 8	49 ± 10	···	FUSE LiF2a
	1142.366	0.633	≤ 21	≤ 21	···	FUSE LiF1b, LiF2a
	1143.226	1.342	26 ± 9	62 ± 12	···	FUSE LiF2a
	1144.938	2.096	72 ± 9	120 ± 16	···	FUSE LiF1b, LiF2a
	1608.451	1.998	112 ± 16	182 ± 29	26 ± 6	HST STIS
Fe III ..	1122.524	2.260	≤ 33	≤ 47	···	FUSE LiF2a, LiF1b

[a]Vacuum wavelengths and oscillator strengths from Morton (1991; 2001, in preparation).

[b]Equivalent widths and 1σ errors (or 3σ upper limits) are listed for Complex C, the IV Arch, and the IVC at +60 km s^{-1} (denoted IV+60).

TABLE 3
ATOMIC COLUMN DENSITIES AND GAS-PHASE ABUNDANCES IN COMPLEX C AND IV ARCH

Species	I.P. [eV]	$\log(X/\mathrm{H})_\odot$ [a] +12	$\log N_{\mathrm{ComplexC}}$ N in [cm^{-2}]	$[X/\mathrm{H}]_{\mathrm{ComplexC}}$ [b]	$\log N_{\mathrm{IVArch}}$ N in [cm^{-2}]	$[X/\mathrm{H}]_{\mathrm{IVArch}}$ [b]
H I	13.60	12.00	19.92 ± 0.01[c]	···	19.48 ± 0.01[c]	···
C II	24.38	8.55	···	···	···	···
N I	14.53	7.97	$13.95^{+0.17}_{-0.21}$	$-1.94^{+0.17}_{-0.21}$	$14.77^{+0.50}_{-0.29}$	$-0.68^{+0.50}_{-0.29}$
N II	29.60	7.97	≤ 15.71	···	···	···
O I	13.62	8.87	$15.77^{+0.37}_{-0.31}$	$-1.03^{+0.37}_{-0.31}$	$16.34^{+0.35}_{-0.27}$	$-0.01^{+0.35}_{-0.27}$
Al II	18.82	6.48	$13.42^{+0.30}_{-0.50}$	$-0.98^{+0.30}_{-0.50}$	···	···
Si II	16.35	7.55	$14.56^{+0.28}_{-0.27}$	$-0.91^{+0.28}_{-0.27}$	$14.81^{+0.28}_{-0.33}$	$-0.22^{+0.28}_{-0.33}$
P II	19.73	5.57	≤ 13.22	≤ -0.27	≤ 13.22	$\leq +0.17$
S II	23.33	7.27	$14.34^{+0.12}_{-0.15}$	$-0.85^{+0.12}_{-0.15}$	$14.86^{+0.11}_{-0.08}$	$+0.11^{+0.11}_{-0.08}$
Ar I	15.76	6.65	≤ 13.15	≤ -1.42	≤ 13.15	≤ -0.98
Fe II	16.16	7.51	$14.16^{+0.20}_{-0.14}$	$-1.27^{+0.20}_{-0.14}$	$14.73^{+0.19}_{-0.15}$	$-0.26^{+0.19}_{-0.15}$
Fe III	30.65	7.51	≤ 13.67	≤ -1.76	≤ 13.86	≤ -1.13

[a] Anders & Grevesse (1989); Grevesse & Noels (1993).

[b] $[X/\mathrm{H}] = \log(N_X/N_{\mathrm{H\,I}}) - \log(X/\mathrm{H})_\odot$, limits are 3σ. Errors do not include an additional 12% uncertainty due to possible sub-structure within the Complex C absorption profiles.

[c] From Effelsberg 21 cm emission line data with a beamsize of 9.′1 centered on PG 1259+593.